A COMPARISON OF THREE CEST IMAGING METHODS

Z. Zu[1], K. Li[1], and D. Gochberg[1]
[1]Radiology, Vanderbilt University, Nashville, TN, United States

Introduction: Chemical exchange saturation transfer (CEST) provides a new imaging contrast mechanism sensitive to labile proton exchange. Potential applications of CEST imaging include cancer, stroke and other human diseases. Three CEST imaging methods (continuous-wave (CW-), pulsed- [1], and spoiled gradient recalled (SPGR-) [2]) are numerically optimized and compared using simulations and a creatine/agarose tissue phantom. We also examine the maximum CEST contrast to noise ratio (CNR), the corresponding normalized CEST contrast, and the optimal average irradiation power as a function of the frequency offset of the agents, exchange rate, and solute concentration in both a two-pool model (water and solute pool) and a three-pool model (water, solute, and macro-molecular pool). Key results include: 1) that the average irradiation power is a more meaningful sequence metric than is the average irradiation field, 2) the simulated optimal average powers are approximately equal to each other in CW and pulsed-CEST imaging for a range of frequency offsets, exchange rates, and solute concentrations when using a two-pool model, but not a three-pool model, 3) that the optimal average power in the three approaches in the two-pool model increases with the frequency offset and exchange rate, but is independent of the solute concentration, 4) that the CNR difference between pulsed- and SPGR-CEST is largely due to conventional gradient-echo and echo planar imaging (EPI) SNR [3] differences.

Methods: CW-, pulsed-, and SPGR- CEST imaging experiments were performed on a creatine phantom (50 mM Creatine plus 3% agarose solution (w/w), pH 6.5) at 9.4T. The sample parameters were determined via a three-pool model fitting of the CW-CEST z-spectrum, and the parameters were then utilized for simulations of the CEST signal by integrating the coupled Bloch equations. CEST CNR defined by Eq [1] was used as a sequence optimization target, since the commonly used CEST contrast defined by Eq [2] produces deceptive and irrelevant results when the non-irradiated signal is small. S(-) and S(+) are the water signals when irradiating at the labile proton resonance and on the opposite side of the water peak, respectively. S_0 is the non-irradiated signal and acquired by performing the CEST sequence without irradiation, and σ is the standard deviation of noise in the image. Additional optimizations were performed with varied CEST agent frequency offset (500 Hz, 1250 Hz, 2000, 3000 Hz), exchange rate (50, 100, 150, 200, 250 Hz), and concentration relative to water (0.001, 0.002, 0.003, 0.004, 0.005). The remaining sample parameters were not changed in these simulations. To analyze the CEST effect without MT, optimizations were also performed using a two-pool model (water and solute pool), in which the concentration of the macro-molecular pool was set to zero.

$$\text{CESTCNR} = \frac{S(+)-S(-)}{\sigma} = \frac{S_0}{\sigma}\cdot\frac{S(+)-S(-)}{S_0} = \text{SNR}\cdot\text{CESTcontra st} \quad [1]$$

$$\text{CESTcontrast} = \frac{S(+)-S(-)}{S_0} \quad [2]$$

Results: Figure 1 plots the optimized square root of the mean square field ($B_{avg\ power}$) and the mean field ($B_{avg\ field}$) as a function of the irradiation flip angle (irradiation FA) and the duty cycle in the simulated pulsed-CEST sequence. $B_{avg\ power}$ is the superior metric for this sample since its optimized value is independent of other acquisition parameters. Figure 2 plots optimal $B_{avg\ power}$ as a function of frequency offset (a), exchange rate (b), and solute concentration (c) in the two-pool model, as well as frequency offset (d) in the three-pool model. Note that the optimum $B_{avg\ power}$ in CW-, and pulsed-CEST imaging is similar in all the two-pool cases, but not in the three-pool case. In addition, the optimal $B_{avg\ power}$ increases with frequency offset and exchange rate, but is independent of the solute concentration. Figure 3 plots simulations of CEST contrast (a) and CEST CNR (b) as a function of the frequency offset. Note that the relative contrast of the SPGR-CEST is much greater than its CNR, which can be explained by the relatively small SNR of conventional gradient-echo imaging.

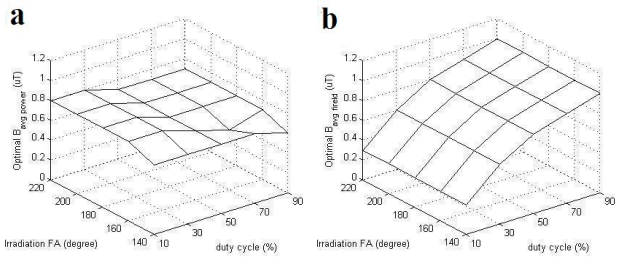

Figure 1: Simulated $B_{avg\ power}$ (a) and optimal $B_{avg\ field}$ (b) that optimize pulsed CEST CNR as a function of irradiation FA and duty cycle.

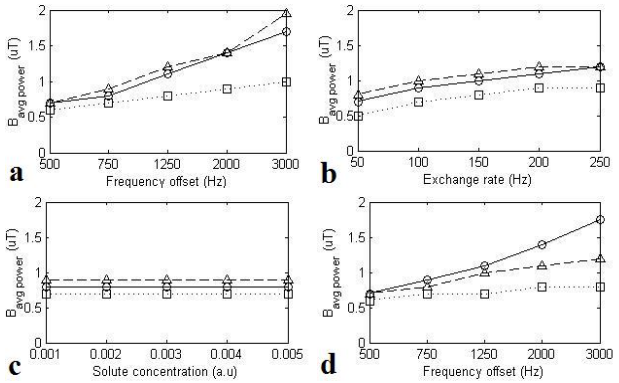

Figure 2: optimal $B_{avg\ power}$ as a function of frequency offset (a), exchange rate (b), and solute concentration (c) in the two-pool model, and frequency offset (d) in the three-pool model. Circle, triangle, and square represent CW, pulsed, and SPGR-CEST, respectively.

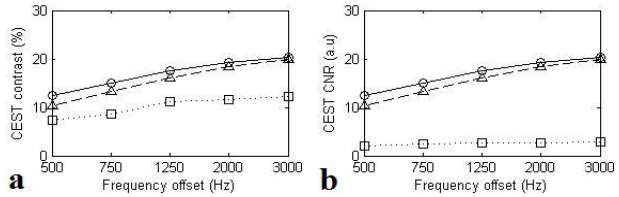

Figure 3: CEST contrast (a) and CNR (b) as a function of frequency offset.

Discussion: SPGR-CEST provides an alternative to the EPI based CW- and pulsed-CEST imaging methods that avoids the artifacts inherent to multi-echo acquisitions, though at the cost of lower CNR.

References:

[1] Sun, P. Z., et al., *Magn. Reson. Med.* 60, 834 (2008)
[2] Desmond, K. L. and Stanisz, G. J., *ISMRM*, 4479, Honolulu, USA (2009)
[3] Haacke, E. M., et al., Magnetic resonance imaging: physical principles and sequence design. (1999)